Eur Biophys J (1987) 14: 263–272

European Biophysics Journal

Three-dimensional structure of deoxycholate-treated purple membrane at 6 Å resolution and molecular averaging of three crystal forms of bacteriorhodopsin

I. N. Tsygannik and J. M. Baldwin***

MRC Laboratory of Molecular Biology, Hills Road, Cambridge CB2 2QH, UK

Received July 7, 1986/Accepted in revised form October 1, 1986

Abstract. The three-dimensional structure of the deoxycholate-treated form of purple membrane has been determined to a resolution of about 6 Å. Using low temperature electron diffraction data, room temperature electron microscope images and improved methods of data analysis, higher resolution has been reached than was obtained using native membranes of the same size. Statistical analysis of the data shows that the new map is considerably better than earlier maps. The map indicates the probable sites for the lipid molecules that remain in the deoxycholate-treated membranes; some of these sites differ from those suggested by the projection map of Glaeser et al. (1985). Comparison of the bacteriorhodopsin structures now determined independently from three crystal forms shows that the monomer structure is independent of the detailed contacts with lipid molecules. The average of the three structures gives a picture with very little noise showing seven similar rod-like features which are clearly best interpreted as α-helices; there is no indication that part of the structure is β-sheet as suggested by Jap et al. (1983). Phases from the averaged structure at 6 Å resolution will enable better refinement of the parameters that will be required in the analysis of higher resolution images from tilted specimens needed to extend the projection map at 3.5 Å resolution (Henderson et al. 1986) to produce a three-dimensional atomic resolution map.

Key words: Bacteriorhodopsin, membrane structure, electron diffraction, electron microscopy, protein-lipid interactions

* To whom offprint requests should be sent
** Current address: Shemyakin Institute of Bioorganic Chemistry, USSR Academy of Sciences, Ul. Miklukho-Maklaya, 16/10, 117871 GSP Moscow, V-437 USSR

1. Introduction

Bacteriorhodopsin (BR) is the only protein in the specialized purple membrane patches of the cell envelope of Halobacterium halobium. It occurs naturally in a well-ordered two dimensional crystal. BR is involved in a photochemical cycle which results in the generation of a transmembrane electro-chemical gradient of hydrogen ions. This can support cell metabolism in an oxygen-deficient environment (Oesterhelt and Krippahl 1983; Stoeckenius et al. 1979). Intrinsic interest in the proton pumping mechanism of BR has encouraged extensive investigations of its chemical sequence (Ovchinnikov et al. 1979, Khorana et al. 1979) and also of its three-dimensional structure in two different crystal forms (Henderson and Unwin 1975; Michel et al. 1980; Leifer and Henderson 1983).

The explanation of the mechanism of action of BR will require detailed information about the structure at atomic resolution. The most powerful method of structure determination, X-ray crystallography, cannot be used in the case of BR because attempts to prepare well-ordered three-dimensional crystals have so far not been successful. Although experimental techniques and software facilities for structural studies of two-dimensional crystals are not so developed as those for X-ray crystallography, it should eventually be possible to obtain an electron density map at worthwhile resolution by using data collection at low temperature and sophisticated methods of data processing (Henderson et al. 1986). It should also be possible to improve the accuracy of maps by combining data obtained from different crystal forms.

This paper reports the analysis in three dimensions to 6 Å resolution of a third crystal form of purple membrane which has trigonal $p3$ symmetry like the native form but which has a cell dimension that is 10% smaller. Treatment of purple membrane

with deoxycholate (DOC) removes a large proportion of the lipids (Hwang and Stoeckenius 1977) and it is possible to retain good crystalline order using the technique of Glaeser et al. (1985). The determination of the projection structure of DOC-treated purple membrane showed that the treatment results in the removal of a layer of lipid molecules from between the BR trimers (Glaeser et al. 1985), replacing protein-lipid interactions by protein-protein contacts in forming the crystal bonds.

The present study was carried out independently of the previous studies of native and orthorhombic two-dimensional crystals of purple membrane, and has produced a map of somewhat higher resolution. The improvement has been achieved mainly by using recently improved methods for data processing of the images (Henderson et al. 1986). Comparison of the new structure from DOC-treated membranes with those from the previous studies allows a more objective assessment of the significance of the features seen in each of the three maps and the average of the maps provides the most noise-free picture of the structure.

2. Materials and methods

a) Structure determination of DOC-treated purple membrane

The DOC-extracted two-dimensional $p\,3$ crystal form of purple membrane was prepared by the method of Hwang and Stoeckenius (1977), modified to produce membrane patches composed of single crystalline domains (Glaeser et al. 1985). The unit cell dimensions of a freshly prepared sample, and of the sample used for the determination of the projection structure by Glaeser et al. (1985), were measured from X-ray diffraction patterns of wet pellets of membranes. They are the same for both samples and are 57.3 Å. The unit cell dimensions of native purple membrane measured by this method are 62.4 Å.

Electron diffraction patterns and low dose images were recorded as described by Glaeser et al. (1985) using crystals of average size 0.5 μm − 0.6 μm. Three-dimensional data were obtained by tilting the specimens by up to 49° for electron diffraction patterns and by up to 63° for images. Processing, merging and curve-fitting of three-dimensional electron diffraction intensity data were carried out in the way described by Leifer and Henderson (1983) and Baldwin and Henderson (1984). Digitized images were processed using procedures which correct for distortions in real space and which take into account contrast transfer function variations across tilted images (Henderson et al. 1986). The use of these procedures allowed higher resolution spots to be detected in the Fourier transforms of the corrected images and enabled precise refinement of focus parameters (amount of defocus in two perpendicular directions and the direction of the astigmatism). Curve fitting to the intensity and phase data was performed using the program LATLINE (Agard 1983).

b) Molecular averaging

Multiple copies of the electron density map of the same protein can be compared and averaged using the suite of programs written by G. Bricogne (1974, 1976). These programs can superimpose and average multiple copies obtained by separate determinations of the structure from different crystal forms as well as those that result from non-crystallographic symmetry within one space group. Essentially the programs determine how to transform coordinates in the unit cell of one crystal form to the corresponding coordinates in the different unit cell. Three crystal forms of BR with different unit cells are available.

The experimental phase data for the map of the native $p\,3$ form were the same as those used for the previously published map (Henderson and Unwin 1975), but the phases were redetermined using the program LATLINE. The amplitudes used in the phase redetermination and also in the map calculation were taken from the electron diffraction data of Baldwin and Henderson (1984). The current native $p\,3$ map is based on 321 structure factors with mean figure of merit 0.95 to a resolution of about 7 Å. Similarly for the orthorhombic form (Leifer and Henderson 1983), the phases were redetermined and the more accurate amplitudes were used to give a map based on 609 structure factors with mean figure of merit 0.85 to a resolution of about 6.5 Å. The DOC map was calculated including 707 structure factors to 5.5 Å, with mean figure of merit 0.87.

The molecular averaging procedure requires that a molecular envelope enclosing a monomer of BR should be defined in each crystal form. For convenience, the map from the orthorhombic form was first superimposed on the map from the native $p\,3$ form, and their average was calculated. Then the map of the DOC form was superimposed on this average map, and the final average calculated giving equal weight to each of the three maps.

The molecular averaging method can be cycled. In such a procedure the averaged map is placed in the correct position and orientation in each of the unit cells, with the space between molecules given a

constant value of density chosen to represent the expected level there. Phases are calculated, and these are combined with the experimental phases and used in the computation of new maps. These maps are the starting point for the next cycle of averaging. The cyclic process is continued until there are no further changes in the calculated phases, when the maps become as similar as possible. This method has proved successful for phase improvement and extension when a sufficient number of copies of the structure have been available (Gaykema et al. 1984; Rossmann et al. 1985; Hogle et al. 1985). Our attempts to improve phase information and to extend it to 5.5 Å were unconvincing when we had amplitude data to 3 Å for the native $p3$ and orthorhombic forms but experimental phase data to only 7 Å and 6.5 Å respectively (Baldwin, unpublished). Our lack of success then seemed to be due mainly to the small number of copies of the structure and, as we now have only one more copy based on phase information to only slightly higher resolution, we considered that the method was still unlikely to help us. The best we can do is to calculate the simple average of the three structures which will give a more accurate final structure and this is what we have done.

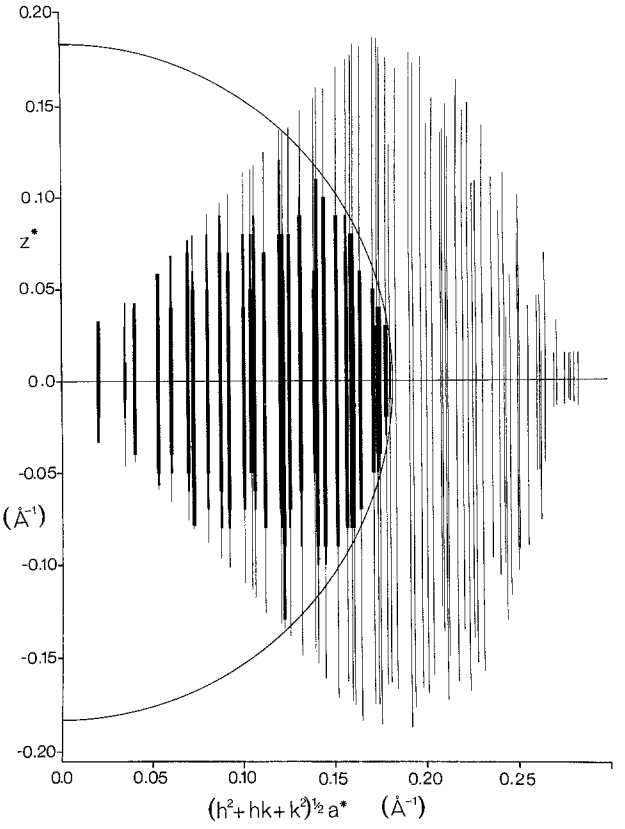

Fig. 1. Extent of the data used in the determination of the structure. The thin lines indicate the regions of z^* for which electron diffraction data were measured for each of the lattice lines out to a horizontal resolution of about 4 Å. The very thick lines indicate the regions of each lattice line for which good phase information was obtained, with figure of merit > 0.85. The lines of intermediate thickness indicate regions for which there was phase information with figure of merit between 0.25 and 0.85. The circle has a radius corresponding to 5.5 Å resolution

3. Results and discussion

a) Electron diffraction data

The best 20% of all the electron diffraction patterns recorded with tilt angles up to 49° were selected visually for subsequent processing and inclusion in the merged three-dimensional intensity data set. The intensities of Friedel-related spots on each pattern were averaged and the quantity R_{sym} was calculated as an indicator of the accuracy of the data. Table 1 shows the mean values of R_{sym} obtained in different ranges of tilt angle. In all, 47 patterns, were used and the data from these were good enough to define the continuous lattice lines of reciprocal space without any large gaps between sampled points, up to a resolution of 4 Å in the plane of the membrane. Inevitably there was a missing cone of data, since the maximum tilt angle obtainable experimentally was 49°. Figure 1 illustrates the extent of the data in z^* for each of the lattice lines for which data were obtained. After fitting damped since functions to the lattice line data and refining parameters for each film against these curves, the consistency of the data was estimated by examining the quantity R_{merge} for each film. Table 1 shows the mean values of R_{merge} obtained in different ranges of tilt angle. As can be

Table 1. Electron diffraction patterns

Tilt angle range [°]	Number of patterns	Number of good spots	Mean R_{sym} [%]	Mean R_{merge} [%]	$\frac{R_{merge}}{R_{sym}}$
0 – 15	15	3,269	7.90	13.02	1.65
15 – 35	14	3,085	12.91	16.28	1.26
35 – 49	18	2,676	20.86	22.42	1.07
All patterns					
0 – 49	47	9,089	13.55	16.98	1.25

$$R_{sym} = \frac{\sum |I_1 - I_2|}{\sum |I_1 + I_2|}$$

where I_1 and I_2 are the intensities of Friedel-related spots on one film

$$R_{merge} = \frac{\sum |I_{obs} - I_{cal}|}{\sum |I_{cal}|}$$

where I_{obs} is the intensity of a spot on one film and I_{cal} is from the curve fitted to the merged data from all films

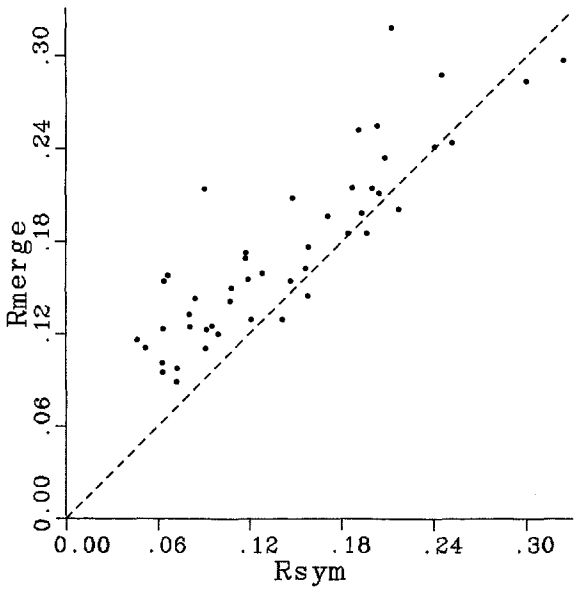

Fig. 2. The plot of R_{merge} against R_{sym} for each electron diffraction pattern. If all errors were entirely random, the *points* would be scattered about a line of slope 1. (See Table 1 for definitions of R_{merge} and R_{sym})

Table 2. Low dose images

Tilt angle range [°]	Number of images	Number of good spots	Number of comparisons	Phase residual [°]
0 – 15	16	1,316	1,199	23.92
15 – 30	16	1,162	1,007	25.58
30 – 45	23	1,303	1,155	26.93
58 – 63	11	308	167	36.24
All images				
0 – 63	66	4,089	3,528	25.96

The interval along the z^*-axis for phase comparison during the final stages of merging and origin refinement was 0.005 $Å^{-1}$

seen from Table 1 and Fig. 2, the R_{merge}/R_{sym} ratio for all patterns used is slightly greater than 1 indicating more disagreement between films than within films. The decrease of this ratio with increase in membrane tilt may result from a larger contribution of random error to the R_{sym} value for tilted patterns which contain weaker and fuzzier spots, whilst other errors are similar for all crystals.

b) Data from electron microscopy

Sixtyone low dose images (about 10% of the images recorded) with tilt angles form 0° to 63° were selected for processing using optical diffraction. Several of the best images among those previously used for the projection structure of the DOC-extracted form of purple membrane (Glaeser et al. 1985) were also included in the merged phase data set. The mean phase residuals between the phases of spots from each image and those of the merged data set are given in Table 2. Judging from these residuals the mean value of the figure of merit for structure factors calculated from the data should be about 0.9.

The data available from the processing of the images do not extend as far in reciprocal space as the intensity data from the electron diffraction patterns, although more images were processed. As the images were taken at room temperature they cannot be expected to give data as good as the diffraction data obtained at near liquid nitrogen temperatures. However the most important reason why data from images is not as good as that from diffraction is explained by Henderson and Glaeser (1985). They concluded that beam-induced specimen movement during the period of radiation damage caused blurring of the image and therefore loss of contrast at high resolution.

The images were initially processed up to a resolution of 4 Å in the plane of the membrane. Although phases for some spots with resolution greater than 5.5 Å were obtained, there were not enough high resolution phases from each image to enable the beam misalignment parameters of the image to be refined satisfactorily and the quality of the phase information to be assessed. Without appropriate correction for the effect of beam tilt the phase information is inaccurate beyond a resolution of about 5.5 Å (Henderson et al. 1986). It was therefore decided not to include phases beyond 5.5 Å in the rest of the analysis.

After combining intensity data from diffraction patterns with phase information from low dose images, curve fitting to the lattice lines was performed using the program LATLINE. The mean figure of merit for the 707 structure factors to 5.5 Å resolution is 0.87 which is similar to the value of about 0.9 expected from the average phase residual (Table 2). The region of reciprocal space in which phase information was obtained is illustrated in Fig. 1. The quality of the data is demonstrated in Fig. 3, which shows four typical lattice lines at different resolutions. In general the phase curves for all lattice lines are much better determined than they were for the previous studies in the other crystal forms because more images were processed and more phases were obtained from each of them. The intensity data are also more accurate than the data used for the previously published maps, being mea-

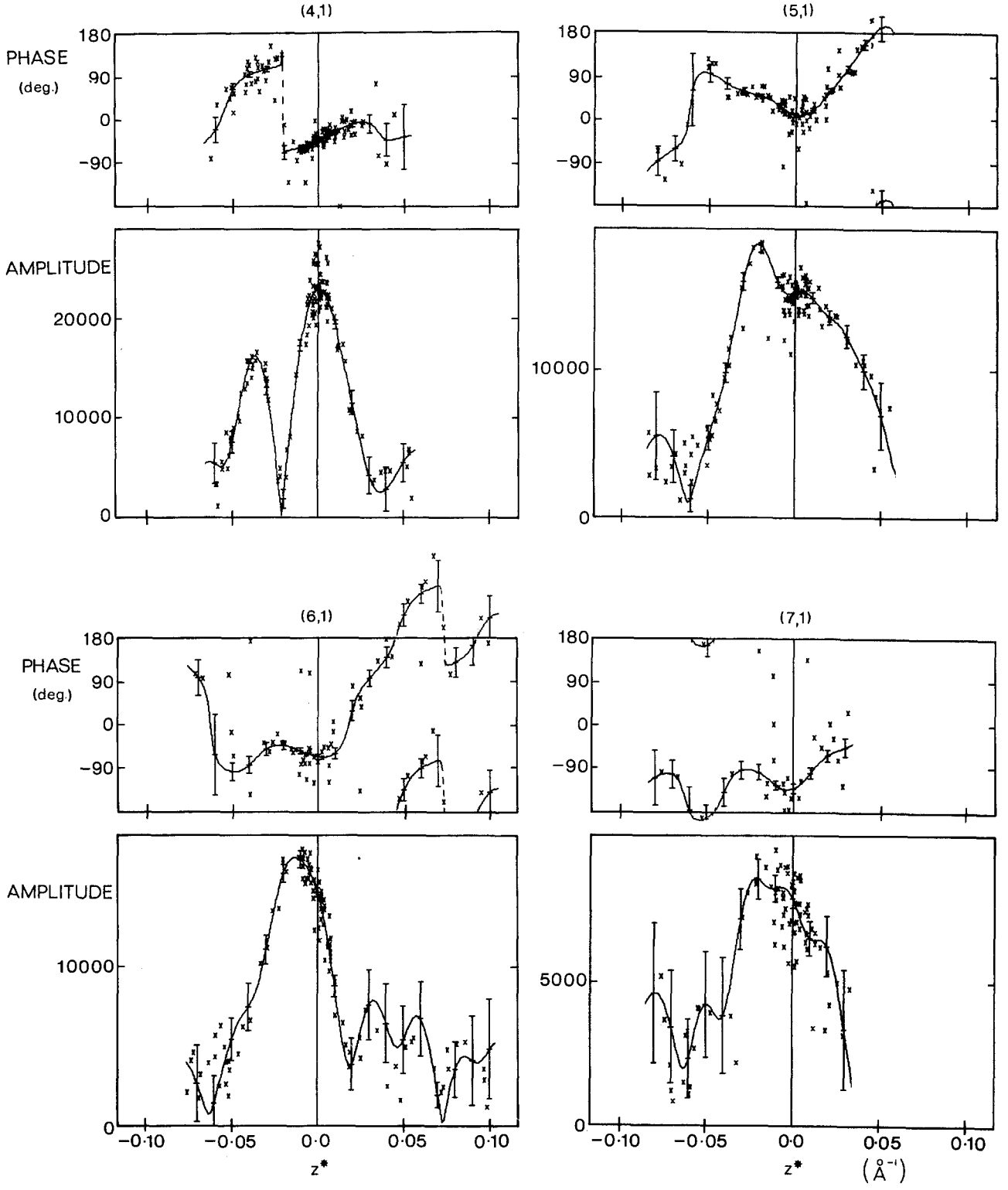

Fig. 3. Experimental data for four lattice lines and the smooth curves fitted to them by the program LATLINE. The *upper part* of each diagram shows the phase data derived from images and the *lower part* shows the amplitude data derived from electron diffraction patterns. The resolutions at $z^* = 0.0$ are 10.8 Å, 8.9 Å, 7.6 Å, and 6.6 Å for the (4, 1), (5, 1), (6, 1) and (7, 1) *lines* respectively. For the *lines* (6, 1) and (7, 1) the resolution at the extreme end of the phase curves is about 6 Å. Amplitudes and phases for the structure factors are extracted from the smooth curves at intervals of 0.01 $Å^{-1}$ in z^*, which gives the required sampling for a unit cell dimension perpendicular to the membrane of 100 Å. The error bars in the phase plot indicate the figures of merit to be given to the structure factors at each sample point; figure of merit = cos (phase error)

sured at low temperature, and there are more data points to define the amplitude curves more accurately.

c) Electron density map

Figure 4a shows the DOC-extracted purple membrane density map with the trimer of BR molecules in the centre. The thickness of the layer containing significant density is about 54 Å (49 Å to 59 Å depending on the choice of contour level). The structure of the trimers is the same as in the native crystal form, confirming the result suggested by the study of the projection structure of DOC-treated purple membrane (Glaeser et al. 1985).

1) Arrangement of lipid molecules. Around the 3-fold axis in the centre of the BR trimer there is enough space for three lipid molecules on both the intracellular (Fig. 4c) and the extracellular (Fig. 4d) sides of the membrane. The central 3-fold axis (type I in Fig. 4b) therefore provides sites for 6 lipids per trimer. Around the outside of each BR trimer there is enough space for lipid molecules near the six 3-fold axes (types II and III in Fig. 4b). The spatial arrangement of the trimers and the slopes of the transmembrane α-helices results in there being space on the extracellular side of the membrane for three lipids around each of these axes. On the intracellular side, however, there is much less room at these 3-folds, particularly at the type II axis. Only one lipid molecule could be accomodated at each axis if the side chains from the neighbouring helices were small, or none if these side chains were large. These sites, 0 to 6 on the top and 18 on the bottom, are shared between 3 trimers, giving sites for 6 to 8 lipids per trimer. The possible total number of lipids per trimer is therefore 12 to 14, 3 to 5 on the intracellular and 9 on the extracellular side (see Table 3). This arrangement of lipid molecules differs somewhat from the arrangement suggested by Glaeser et al. (1985) from their study of the projection.

There is some indication of density for lipid molecules on the intracellular side of the membrane (Fig. 4c). There are three density peaks around the 3-fold axis of type I and one peak on each of the 3-fold axes of types II and III. On the extracellular side (Fig. 4d), there are three small peaks around the trimer type I axis but no others.

2) Structure of the BR monomer. As can be seen in the density map (Fig. 4a) each BR molecule in the trimer shows the same seven rod-like features found in the earlier analyses of native (Henderson and Unwin 1975) and orthorhombic (Leifer and Henderson 1983) forms of purple membrane. A surface representation of the BR monomer is shown in Fig. 5a. The high density and the shape of the rods suggest that they are trans-membrane α-helices. All the α-helices are about the same length and have different inclinations with respect to the normal to the membrane plane. Helix 1 appears to have a kink in the middle of it that divides it into two parts of nearly equal length and nearly equal inclination to the membrane plane. Helix 1 also had this appearance in the map from the orthorhombic form. The resolution of the map, although slightly higher than that of previous maps, is still not sufficient to show clear connecting links between the helices.

3) Molecular averaging. The new map is based on significantly more data than was present in the previously determined maps. Table 4 summarises the amount and quality of the data that is presented in each map. The new data clearly improve the quality of information we have to describe the structure to 6 Å resolution, and the DOC data extend to higher resolution than was available before. The main reason for this is the improved method of

Table 3. Possible arrangement of lipid molecules in DOC-extracted purple membrane

Membrane surface	Number of lipids at 3 different types of 3-fold axis surrounding one trimer			Total per trimer
	I[a]	II[a]	III[a]	
Intracellular	3	0 or 1	0 or 1	3, 4 or 5
Extracellular	3	3	3	9
Both sides	6	3 or 4	3 or 4	12, 13 or 14

[a] See Fig. 4b for definition of types of 3-fold axes

Table 4. Number of measured structure factors for each of the three maps

Resolution range [Å]	Native *p*3			Orthorhombic			DOC		
	Number	Mean fom	%	Number	Mean fom	%	Number	Mean fom	%
100.0–7.0	314	0.96	45	472	0.86	57	390	0.90	66
7.0–6.5	7	0.92	4	69	0.82	37	79	0.87	53
6.5–6.0				68	0.80	26	102	0.88	53
6.0–5.5							136	0.81	50

fom = figure of merit

$$\% = 100 \frac{\text{(number of observed structure factors)}}{\text{(total number in resolution range)}}$$

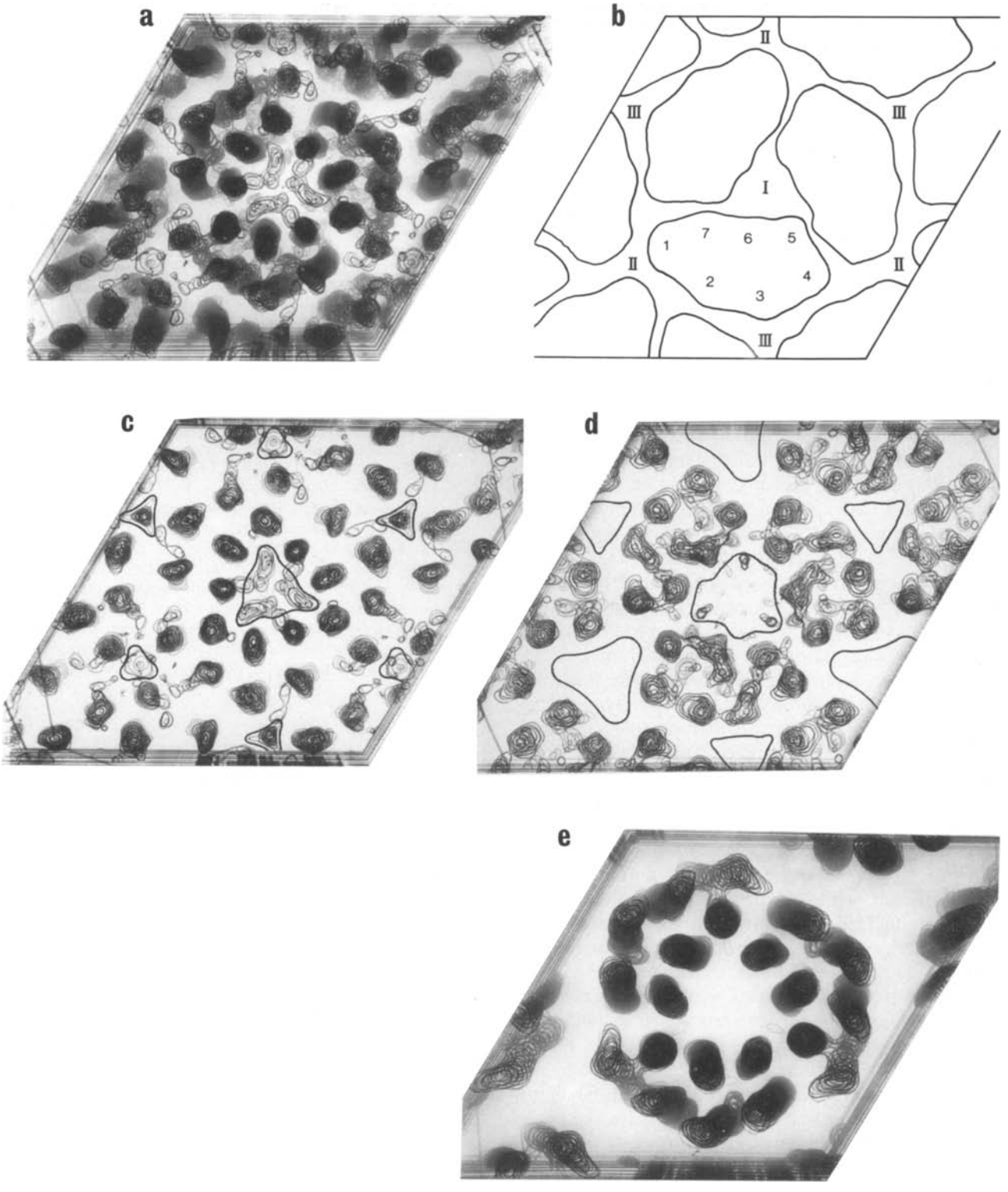

Fig. 4. **a** The density map of DOC-extracted purple membrane showing a trimer of BR molecules. The view is from the cytoplasmic side of the membrane and the depth through the map shown is 54 Å. The density at the first contour drawn is 15% of the maximum density in the map and the interval between contours is 10% of the maximum density. **b** The outline of the monomers in the central and surrounding trimers. The numbering of the α-helices, 1 to 7 as in Engelman et al. (1980), is shown for one monomer. The three distinct types of crystallographic 3-fold axes are labeled I, II and III. **c** The top 15 Å of the map. **d** The bottom 15 Å of the map. The direction of view for **c** and **d** is the same as in **a**. The space available for lipid molecules is indicated by the boundaries drawn around the 3-fold axes in **c** and **d**; possible density for the lipids can be seen within some of these boundaries. **e** The average of the maps from the native *p* 3, orthorhombic and DOC-treated crystal forms showing a trimer of BR molecules replaced in the native *p* 3 unit cell. The contouring scheme is the same as for **a, c** and **d**

image processing that now includes the removal of distortions from the images (Henderson et al. 1986).

The DOC map was compared to the previously determined maps from the native $p\,3$ form and from the orthorhombic form, using the suite of programs written by G. Bricogne (1974, 1976) for finding the best superposition between multiple copies of the same protein structure. The results from the least squares comparisons between the electron densities from the three crystal forms are summarised in Table 5. When the maps are optimally superimposed, the correlation coefficients between all pairs of maps are greater than 0.67. The parameters that describe how to superimpose the molecules in the three unit cells are given in Table 5. Once the three maps were correctly superimposed, the electron densities were averaged, with the reconstituted averaged map placed in the native $p\,3$ unit cell, with an appropriate constant value of density between the molecular envelopes (see Fig. 4e).

The molecular replacement programs can be used to demonstrate the relative accuracy of the data in the three original maps and in the average map. We now have a very accurate set of projection phases to 3.5 Å resolution for the native $p\,3$ form of BR (Henderson et al. 1986). We are able to compare the phase information in the original native $p\,3$, orthorhombic and DOC data sets with this new projection data as follows. The electron density corresponding to a protein monomer was extracted from each original map and was placed in the three correct positions in the native $p\,3$ unit cell with a constant level of density in the space between the molecular envelopes. The phases calculated from the maps reconstituted in this way sample the phase information of the original maps at points that can be compared with the new native $p\,3$ data. The mean phase residuals between the new projection data and the corresponding values from the three original data sets are shown in Table 6, along with the phase residual obtained with the phases from the average map. It can be seen that the DOC data is clearly superior to that from the original native $p\,3$ and orthorhombic studies out to 6 Å resolution. To 7 Å resolution the average of the three maps gives better phases than do the three maps separately, and to 6 Å resolution it gives phases of the same accuracy as those from the DOC data. The calculated phases beyond 7 Å from the native $p\,3$ reconstituted map come almost entirely from phase extension due to flattening the density in the space between the molecules. Similarly calculated phases beyond 7 Å from the map reconstituted from orthorhombic data and beyond 6 Å from the map reconstituted from DOC data are influenced by phase extension to some extent. The phase residuals in the resolution range 6 Å to 5.5 Å are not statistically significant because of the small number of spots for comparison, so we cannot assess the quality of the DOC phase information in this resolution range. However, we can be sure that the DOC data are reliable to 6 Å resolution.

Figure 4e illustrates the averaged structure of BR as it would appear in the trimer of the native $p\,3$ form. The average map is less noisy than the map of the DOC form seen from the same viewpoint in

Table 5. 1) Superposition of BR molecules in three crystal forms

	Correlation C	Depth compared [Å]
Native $p\,3$ and ortho	0.71	56.6
Native $p\,3$ and DOC	0.77	56.6
DOC and ortho	0.67	54.5

$$C = \frac{\sum \varrho_1 \varrho_2 - (\sum \varrho_1 \cdot \sum \varrho_2)/n}{[\sum \varrho_1^2 - (\sum \varrho_1)^2/n]^{1/2} \cdot [\sum \varrho_2^2 - (\sum \varrho_2)^2/n]^{1/2}}$$

2) Translational and rotational parameters describing superposition

Comparison	X	Y	Z	θ_1	θ_2	θ_3	$\theta_1+\theta_3$
Native $p\,3$ and DOC	0.00	0.00	−4.40	2.2	0.0	−1.0	1.2
Native $p\,3$ and ortho	35.67	54.71	−5.30	6.35	2.17	24.62	30.97

This table gives the relationship between BR molecules after the best superposition has been found. X, Y, Z are the coordinates in Å of the origin of the native $p\,3$ unit cell refered to the x, y^*, z axes of the DOC or orthorhombic unit cells. θ_1, θ_2, θ_3 are the standard Eulerian angles in degrees that describe the rotations to apply to the x, y^*, z axes of the DOC or orthorhombic cells to superimpose them on the x, y^*, z axes of the native $p\,3$ cell. When θ_2 is zero or very small, $\theta_1+\theta_3$ is a useful parameter describing the rotation around the z axis

Table 6. Phase residuals against 'new' native $p\,3$ projection data

Resolution [Å]	Number of comparisons	Phase residuals [°]			
		Native $p\,3$ [a]	Ortho [a]	DOC [a]	Average [a]
15.0–7.0	28	22.5	19.7	13.9	12.8
7.0–6.0	15	61.3	56.5	36.7	42.9
6.0–5.5	8	71.6	58.0	87.1	70.1

[a] Residuals between the entirely independent new native $p\,3$ projection phases (Henderson et al. 1986) and phases calculated from maps reconstituted in the native $p\,3$ unit cell from molecular densities taken out of the three separate original maps and from the averaged map

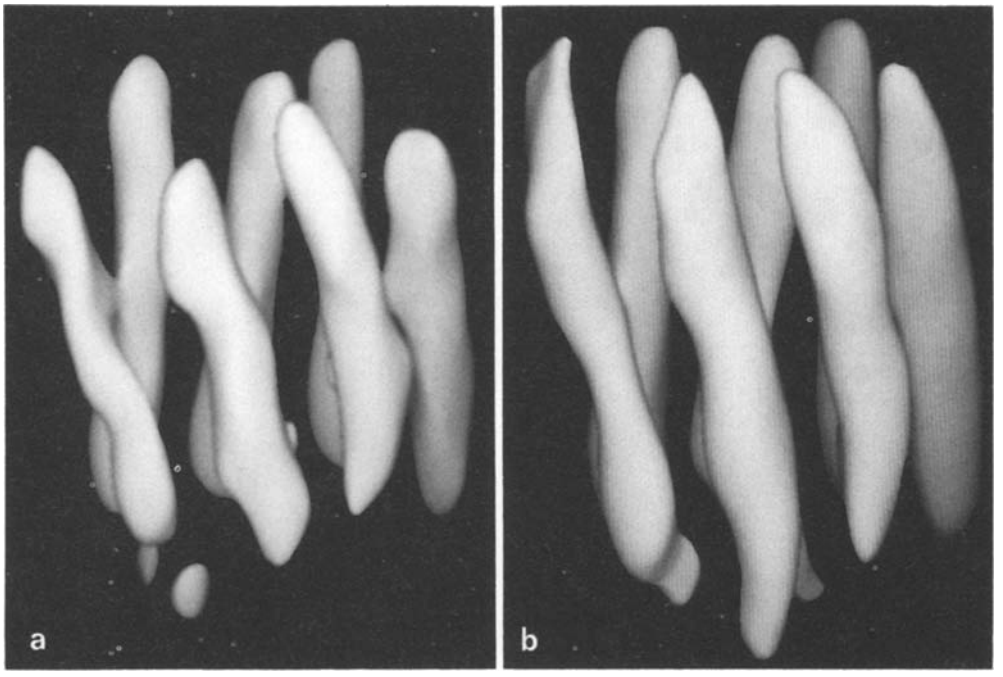

Fig. 5. Surface representation of a single BR molecule. **a** The DOC-treated purple membrane structure. The surface represented is that of the second contour level of Fig. 4a. **b** The best current estimate of the structure produced by averaging the maps from the native *p* 3, orthorhombic and DOC-treated crystal forms. The surface represented is that of the first contour level in Fig. 4e. The views in **a** and **b** are the same with helices 1 to 4 in the foreground and the cytoplasmic surface at the top. (A program written by G. Vigers was used to produce these pictures from the density maps)

Fig. 4a. A surface representation of the averaged monomer and a similar view of the monomer determined from the DOC crystal form are shown in Fig. 5. The resolution of the averaged map is essentially only 6 Å and no connections between helices are visible. But this map provides the most reliable estimate of what the structure looks like at this resolution. All the helices have similar density and there is no indication that helices 1 and 2 could be β-sheet as suggested by Jap et al. (1983). Four strands of β-sheet instead of two helices would not have density concentrated into two rod-like features, but would have a lower density spread evenly through the region. The structure of BR is clearly best interpreted as seven transmembrane α-helices.

Acknowledgements. We are grateful to Richard Henderson for help and encouragement throughout this work and to Thomas Ceska for many useful discussions. Igor Tsygannik was supported by the USSR Academy of Sciences.

References

Agard DA (1983) A least-squares method for determining structure factors in three-dimensional tilted-view reconstructions. J Mol Biol 167:849–852

Baldwin J, Henderson R (1984) Measurement and evaluation of electron diffraction patterns from two-dimensional crystals. Ultramicroscopy 14:319–336

Bricogne G (1974) Geometric sources of redundancy in intensity data and their use for phase determination. Acta Crystallogr A30:395–405

Bricogne G (1976) Methods and programs for direct-space exploitation of geometric redundancies. Acta Crystallogr A32:832–847

Engelman DM, Henderson R, McLachlan AD, Wallace BA (1980) Path of the polypeptide in bacteriorhodopsin. Proc Natl Acad Sci USA 77:2023–2027

Gaykema WPJ, Hol WGJ, Vereijken JM, Soeter JM, Bak HJ, Beintema JJ (1984) 3.2 Å structure of copper-containing, oxygen-carrying protein Panulirus interruptus haemocyanin. Nature 309:23–29

Glaeser RM, Jubb JS, Henderson R (1985) Structural comparison of native and deoxycholate-treated purple membrane. Biophys J 48:775–780

Henderson R, Glaeser RM (1985) Quantitative analysis of image contrast in electron micrographs of beam-sensitive materials. Ultramicroscopy 16:139–150

Henderson R, Unwin PNT (1975) Three-dimensional model of purple membrane obtained by electron microscopy. Nature 257:28–32

Henderson R, Baldwin JM, Downing KH, Lepault J, Zemlin F (1986) Structure of purple membrane from Halobacterium halobium: recording, measurement and evaluation of electron micrographs at 3.5 Å resolution. Ultramicroscopy 19: 147–178

Hogle JM, Chow M, Filman DJ (1985) Three-dimensional structure of Poliovirus at 2.9 Å resolution. Science 229: 1358–1365

Hwang S-B, Stoeckenius W (1977) Purple membrane vesicles: morphology and proton translocation. J Membr Biol 33: 325–350

Jap BK, Maestre MF, Hayward SB, Glaeser RM (1983) Peptide-chain secondary structure of bacteriorhodopsin. Biophys J 43:81–89

Khorana HG, Gerber GE, Herlihy WC, Gray CP, Anderegg RJ, Nihei K, Bieman K (1979) Amino acid sequence of bacteriorhodopsin. Proc Natl Acad Sci USA 76:5046–5050

Leifer D, Henderson R (1983) Three-dimensional structure of orthorhombic purple membrane at 6.5 Å resolution. J Mol Biol 163:451–466

Michel H, Oesterhelt D, Henderson R (1980) Orthorhombic two-dimensional crystal form of purple membrane. Proc Natl Acad Sci USA 77:338–342

Oesterhelt D, Krippahl G (1983) Phototrophic growth of Halobacteria and its use for isolation of photosynthetically-deficient mutants. Ann Microbiol (Paris) 134B: 137–150

Ovchinnikov YuA, Abdulaev NG, Feigina MYu, Kiselev AV, Lobanov NA (1979) The structural basis of the functioning of bacteriorhodopsin: an overview. FEBS Lett 100: 219–224

Rossmann MG, Arnold E, Erickson JW, Frankenberger EA, Griffith JP, Hecht HJ, Johnson JE, Kamer G, Luo M, Mosser AG, Rueckert RR, Sherry B, Vriend G (1985) Structure of a human common cold virus and functional relationship to other picornaviruses. Nature 317:145–153

Stoeckenius W, Lozier RH, Bogomolni RA (1979) Bacteriorhodopsin and the purple membrane of halobacteria. Biochim Biophys Acta 505:215–278

Unwin PNT, Henderson R (1975) Molecular structure determination by electron microscopy of unstained crystalline specimens. J Mol Biol 94:425–440